Ultra-Compact Integrated Coherent Receiver for High Linearity RF Photonic Links

Uppiliappan Krishnamachari, Sasa Ristic, Anand Ramaswamy, Leif A. Johansson, Chin-Hui Chen, Jonathan Klamkin, Molly Piels, Ashish Bhardwaj, Mark J. Rodwell, John E. Bowers, Larry A. Coldren

Electrical and Computer Engineering Department
University of California, Santa Barbara
Santa Barbara, CA, U.S.A

ukrishna@ece.ucsb.edu

***Abstract*—We demonstrate a novel photonic integrated circuit(PIC) that combines an ultra compact trench beam splitter with monolithically integrated photodetectors and modulators. A coherent receiver is realized by flip chip bonding of this PIC with an electronic integrated circuit (EIC). Preliminary system results yield a third-order intermodulation distortion suppression of 46 dB at a signal frequency of 300 MHz.**

I. INTRODUCTION

Analog optical links are commonly used in the transmission of signals to and from remote antennas and electrical sensors. Since these links are designed to convey a wide range of signals, high-linearity and low-noise operation are required to retain the fidelity of the input signal. The emphasis of this work is on the receiver end of the link which currently poses the greatest challenge in terms of system linearity requirements [1].

In traditional intensity modulated direct detection (IMDD) photonic links, the dominant limitation on dynamic range is the relative intensity noise of the optical source, which is proportional to the square of the average optical power [2]. Furthermore, the modulation depth of MZM-based IMDD systems is limited to 100%. In contrast, phase modulated (PM) optical links can employ $LiNbO_3$ phase modulators that can be driven through many π phase shift, providing a clear advantage in terms of link dynamic range. Use of balanced detection in coherent systems diminishes relative intensity noise (RIN), enabling systems that approach shot noise limited performance [3].

Similar to an IMDD link, a coherent link still employs an interferometer, with an inherently non-linear, sinusoidal transfer function. To overcome this limitation, we have previously proposed a coherent optical receiver that uses negative feedback to suppress the nonlinearities inherent to the phase demodulation process [4]. The receiver architecture is shown in Figure 1. The phase modulated signal from the transmitter is mixed with the signal output of the feedback reference phase modulator. Optical mixing is achieved by using an interferometer followed by a balanced detector pair. The balanced PD produces an error signal that is amplified, filtered, and fed back to the reference phase modulator to compensate the phase difference between the signal and local oscillator. This effectively lowers the signal swing of the demodulator thereby restricting the operation of the receiver to the linear region of the response curve.

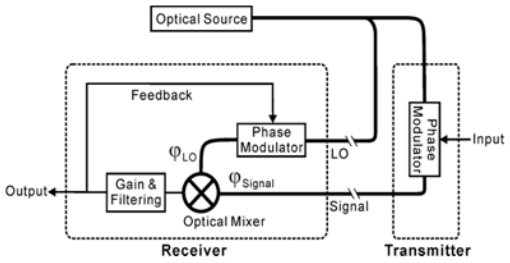

Figure 1: Architecture of coherent receiver with feedback

II. DEVICE DESIGN AND FABRICATION

Because of bandwidth limitation due to latency in the loop, the delay must be kept short for stable operation at high frequencies. Monolithic integration of the receiver components is necessary to limit the loop delay and maximize the optical power coupled to the PDs by avoiding additional coupling losses. We have designed several iterations of PICs that monolithically integrate balanced photodetector pairs, phase modulators and 2x2 combiners on an InP platform. To realize a large loop bandwidth, the capacitances of photodiodes and modulators are exploited as circuit elements to perform the desired loop integrations in the feedback path [5]. Uni-travelling-carrier photodiodes (UTC-PDs) are employed for the balanced PDs because of their high photocurrent operation made possible by reduced space charge effects [6]. The device is designed in a push pull

This material is based upon work supported by the DARPA-PHOR-FRONT program under United States Air Force contract number FA8750-05-C-0265

978-1-4244-7825-5/10/$26.00 ©2010 IEEE

Layer	In (%)	As (%)	Thickness (nm)	Doping (cm^{-3})
InP	100	0	150	1E18
InGaAs	53.2	100	75	P
InGaAs	53.2	100	8	UID
InGaAsP	75.85	52.34	16	UID
InP	100	0	6	UID
InP	100	0	7	1E18
InP collector	100	0	200	N
InP field termination	100	0	25	2E18
InGaAsP stop etch	71.14	61.12	15	UID
InP regrowth	100	0	15	UID
InGaAsP waveguide	71.14	61.12	55	1E17
InGaAsP Barrier	71.54	58.86	25	UID
14x InGaAsP Barrier	71.54	58.86	8	UID
15x InGaAsP QW	71.54	77.53	6.5	UID
InGaAsP Barrier	71.54	58.86	25	UID
InGaAsP waveguide	71.14	61.12	55	1E17
n-InP	100	0	600	1E18
n-InGaAsP contact	85.47	31.72	100	3E18
n-InP	100	0	500	1E18
SI InP substrate	100	0	350,000	8E18 - 3E19

TABLE I. Device Epitaxial Structure

configuration with symmetric tracking phase modulators used to cancel even order distortion terms [3]. In [4], a 2x2 multimode interference (MMI) coupler was used as the mixing element. That PIC was wirebonded to an external EIC that provided transconductance amplification of the feedback signal. In the present iteration, we aim to reduce the loop delay of the original design by utilizing an ultra compact trench beam splitter to reduce the footprint of the PIC. This condensed PIC is then flip chip bonded to the EIC, thereby avoiding the delay of the wirebonds and reducing the delay of the on-chip wiring.

The monolithic integration platform for the coherent receiver is realized on a semi-insulating InP substrate and requires a single regrowth step to form modulator, photodetector, and passive regions. The epitaxial structure, shown in Table 1, consists of the UTC-PD structure grown on top of unintentionally doped (UID) InGaAsP modulator QWs and barriers. The optical waveguide consists of a multiple quantum well (MQW) stack of 15 compressively strained wells and 16 tensile strained barriers [4]. The QW width is 65 Å and the barrier width is 80 Å.

Photodetection regions are formed by selectively removing the UTC-PD layers. This is followed with a p-cladding and p-contact regrowth. The optical waveguide uses a dry-etched deep ridge architecture to allow the flexibility of device geometry that the trench coupler requires. Comparatively, in surface ridge architectures, any features oriented significantly off the major plane suffer severe crystallographic undercut in the wet-etching process [7].

Waveguides and modulators are defined using a dual mask of 55 nm Cr and 500 nm SiO_2, and are deeply etched using Cl_2:H_2:Ar chemistry in an ICP-RIE system. Very low passive waveguide loss of 2.2 cm^{-1} has been reported for this deep etching process [8]. Next, mesas are etched to expose the underlying n-contact layer. The InGaAs p+ contact layer is selectively removed between contacts to provide electrical isolation, and n- and p-contacts are deposited and annealed. In order to minimize diode series resistance of the modulators and the detectors, we first deposit a pre-metal layer which is a very thin stack of Pt/Ti/Pt/Au. This liftoff is carried out in such a way that the top p-side contact layer is not exposed until just before the metal deposition. This method largely avoids contamination of the metal-semiconductor interface, which is an important factor in achieving low diode resistance. Modulators of 500 µm length are defined in the metal deposition steps.

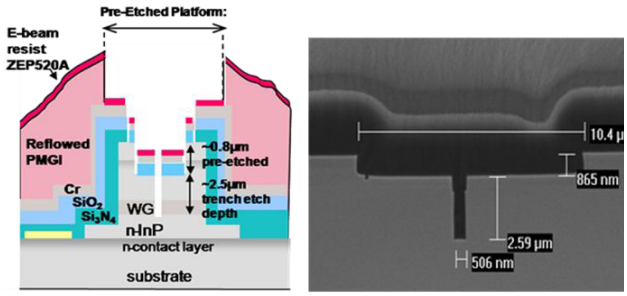

Figure 2(a). Trench planarization process. (b) Cross-sectional SEM of trench

The passive portions of the waveguide are proton implanted to reduce optical loss. To realize the balanced PD configuration, a series of high energy implants ranging from 40 keV to 1.275 MeV are used to electrically isolate the n-contact layer. Transmission line model (TLM) measurements yield an implanted sheet resistance of 4.8 MΩ/square on the n-material and 1.9 MΩ/square on the p-material. The PDs can then be connected in series with minimal electrical cross talk between the diodes.

The trench coupler is designed to act as a frustrated total internal reflection (FTIR) mirror, reflecting and transmitting equal parts to the photodetectors. The input waveguide is incident on the FTIR mirror at an angle greater than the critical angle. Normally this should result in a fully reflected wave, but designing a narrow enough trench allows evanescent coupling of the incident wave across the trench that can result in an ultra compact 50:50 beam splitter. Benzocyclobutene(BCB) with a refractive index of 1.57 is used to fill in the trench. With a calculated effective index of 3.265 for the waveguide, the critical angle is 28.5^0. Crossing angles in the range of 27^0-32^0 were fabricated, correlating to trench widths of 0.25-0.5 µm. Trenches were written using electron beam lithography (EBL). Because ZEP-520 e-beam resist is very thin (~3000 Å), the topography of the sample (which has waveguides over 3µm high) makes it very challenging to get the necessary sidewall coverage over a large step and provide a robust trench etch mask. Furthermore, the minimum thickness of the SiO_2 dielectric mask is 6000 Å, which is far too much to be etched using the thin e-beam resist. Therefore, a planarization process, using Polymethylglutarimide (PMGI) resist is employed. By reflowing the PMGI at 275^0C for 20 min, the step height is reduced from 3.1 µm to 1.2 µm, which is within the step coverage tolerance of the e-beam resist. In order to reduce the required etch depth to reach the waveguide, a wider region around the trench is pre-etched down by ~1 µm.

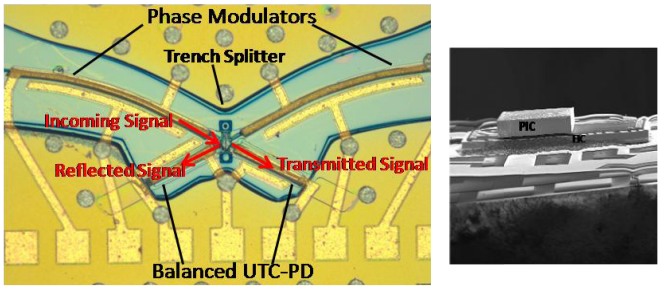

Figure 3(a): Top View of PIC. (b) Side view of flip chip bonded PIC + EIC

*S*imulations show that the effective index of the waveguide changes very little as a result of this pre-etching.This reduces the target etch depth to about 2 µm which is possible for the designed trench widths. A diagram of the pre-etching, planarization, and subsequent trench etch processes is shown in Figure 2(a). A dual layer mask of Cr/SiO_2 is used as the trench hard mask. Both the pre-etch and the trench etch itself utilize the Cl_2:H_2:Ar chemistry used for the waveguide etch. Gas flows, pressure, and ICP power were varied to optimize the trench for depth, sidewall straightness and smoothness, resulting in a high aspect-ratio trench coupler. A cross-sectional SEM of the optimized trench etch is shown in Figure 2(b). After the trench etch, thick pad metal is deposited using an angled, rotating stage to ensure step coverage of the metal. A top view of the completed PIC is shown in Figure 3(a).

The last step of device fabrication is the integration of the transconductance amplifier EIC to the coherent receiver PIC by flip-chip bonding. After thick pad metal is deposited for the contacts, flip chip vias are opened and 2 µm tall Indium bumps are deposited to provide the contact points between the diodes of the PIC and the EIC connections. The PIC and the EIC are carefully aligned and bonded at a force of 1000 g and a temperature of 200^0C. An SEM of the final integrated flip-chip bonded coherent receiver is shown in Figure 3(b).

III. INTEGRATED RECEIVER RESULTS

The total delay includes the delay incurred by the PIC, the EIC and the interconnections between them. In the MMI-based device reported in [4], the total loop delay was ~27 ps, where a significant portion of the delay was caused by the wirebond interconnects. In comparison, the ultra-compact trench-based flip-chip bonded approach used in this work reduces the loop delay to ~10 ps. This is expected to increase the stable open loop gain by 20 dB at 1 GHz, the target frequency of operation [9].

The pre-metal deposition process described in the previous section decreases the forward diode resistance by a factor of 6. The measured diode resistance in forward bias is ~5 Ω for 300 µm x 3 µm modulators and ~20 Ω for 50 µm x 7 µm detectors. Using a test electronic chip with direct traces to each diode contact, the PIC diode characteristics were measured before and after flip- chip bonding. In most cases, the diode series resistance improved after flip chip bonding, perhaps because the In bumps make more stable contacts than the pin probes used to test the diodes prior to bonding.

The efficiency and loss were measured for phase modulators that were separately fabricated using the same quantum well and waveguide structures used in this PIC [10]. For a 500 µm long modulator, the V_π was measured to be 3.9 V. The loss incurred between 0 V and V_π was 5.5 dB. The normalized PD response shows a 3dB bandwidth of ~5 GHz for a 7 µm x 150 µm device at -4 V bias. This bandwidth is more than satisfactory for our link experiments carried out at 300 MHz. Saturation and linearity measurements of the UTC-PDs were reported in [4]. Saturation current, defined as the photocurrent level where the RF response is compressed by 1 dB, is reported to be 80 mA at a bias of -3 V. The third order output intercept point(OIP3), which is a measure of PD linearity, was found to be 46 dBm at 60 mA of DC photocurrent. The high performance of these UTC-PDs indicates that we can achieve high open loop gain without creating nonlinearities.

The trench coupler splitting ratio was tested under illumination from a laser source emitting at 1548.51 nm. Light was fiber coupled into a phase modulator, split into reflected and transmitted waves at the trench, and detected at the UTC-PDs. A polarization controller was utilized to characterize the trench coupler for both TE and TM polarizations. For many of the trench designs implemented, the measured TE splitting ratio was very close to 50:50, with about 1.2 mA into each detector at an input power of 10 dBm at the device facet. The detected TM photocurrent for the same device was 2 mA and 0.4 mA for the reflected and transmitted waves, respectively.

To characterize the mixing efficiency, we send a local oscillator signal to both phase modulator inputs and apply phase modulation to one arm. The signal in the photodetectors will swing as the two input signals drift in and out of phase with each other. If we subtract the signals of the series connected photodetectors, we get the balanced detector signal. Following the derivation in [11], and assuming ideal balanced detection, the maximum amount of coherent mixing corresponds to a balanced detector signal swing of 4 x (average photocurrent in each detector). In the non-ideal case, there will be a coherence penalty due to imbalance in power coupled to each arm, imbalanced splitting ratio, polarization mismatch and wavefront mode mismatch between the reflected and the transmitted beam.

An oscilloscope trace of the balanced detector signal is shown in Figure 4. The voltage swing of the individual photodetector signals, $V_1(t)$ and $V_2(t)$ are shown in the top and bottom traces. The middle trace is (V_1-V_2), the balanced photodetector signal. The maximum observed signal swing for the device tested in Figure 4 was found to be 524 mV with an average I_{DC} of 3.5 mA into each detector. Considering the 50 Ω input impedance of the oscilloscope, the maximum possible signal swing is 700 mV. Thus the coherence efficiency of the mixer is ~75%.

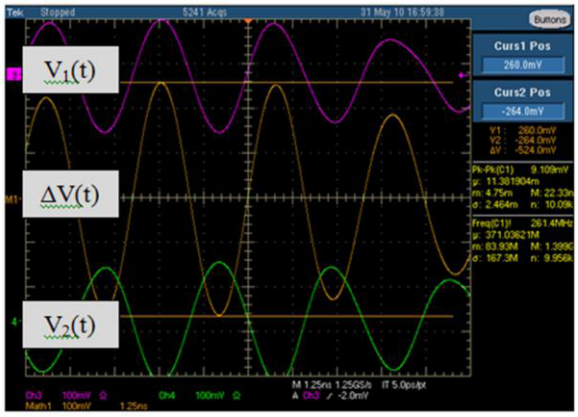

Figure 4: Measurement of Coherent Mixing in Balanced Photodetector

The suppression of the receiver nonlinearity is characterized for the full flip-chip bonded PIC + EIC. Two-tone measurements were carried out at signal frequencies of 298 MHz and 300 MHz. Output frequency spectra of the receiver with and without the use of the feedback loop are shown in Figure 5. The input power was 0 dBm per tone. The IMD3 term is suppressed by an additional 46 dB when the feedback loop is in operation, showing that the system does indeed suppress receiver nonlinearity. Assuming a shot-noise limited optical source, the calculated SFDR would be 122 $dB \cdot Hz^{2/3}$. For detailed discussion of SFDR characterization, see [9].

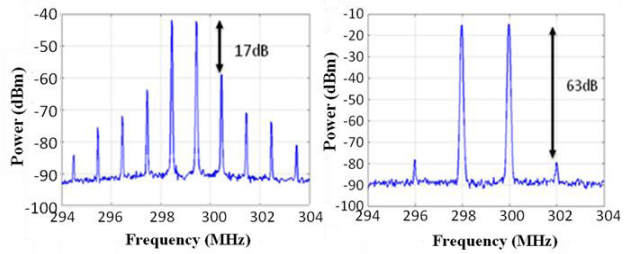

Figure 5: Measured IMD3 suppression with and without feedback loop

IV. CONCLUSION

Design and fabrication of a coherent receiver with feedback was presented. Flip chip bonding of the PIC to the EIC was used to reduce feedback latency. Trench beam splitters were developed to enable an ultra-compact PIC. We have achieved a very low latency feedback loop. Suppression of IMD3 by 46 dB was achieved.

ACKNOWLEDGMENT

The authors would like to thank Roy Yoshimitsu, Dennis W. Scott and Rich Davis of Northrop Grumman Aerospace Systems(NGAS) for designing and fabricating the EIC. Many thanks to Ron Esman for useful contributions and discussions. This work was supported by DARPA-MTO under the Phorfront program.

REFERENCES

[1] L.A. Johansson, H.F. Chou, A. Ramaswamy, J. Klamkin, L.A. Coldren, M.J. Rodwell and John E. Bowers, "Coherent Optical Receiver for Linear Optical Phase Demodulation." *IEEE MTT-S International Microwave Symposium (Invited),* Honolulu, Hawaii, 2007.

[2] D. A. I. Marpaung, C. G. H. Roeloffzen, W. van Etten, "Characterization of a Balanced Modulation and Detection Analog Optical Link," *Proceedings of the 12th Annual Symposium of the IEEE/LEOS Benelux Chapter*, Brussels, Belgium, 17-18 December 2007, pp. 255-258.

[3] J. Klamkin, L.A. Johansson, A. Ramaswamy, N. Nunoya, S. Ristic, U. Krishnamachari, J. Chen, J. E. Bowers, S. P. DenBaars, L.A. Coldren, "Highly Linear Integrated Coherent Receivers for Microwave Photonic Links," *Optical Fiber Communication (OFC) (invited),* paper no. OMK4, San Diego, CA, 2009 S

[4] H. F. Chou, A. Ramaswamy, D. Zibar, L.A. Johansson, L. Coldren and J. Bowers, "SFDR Improvement of a Coherent Receiver Using Feedback," in Optical Amplifiers and Their Applications/Coherent Optical Technologies and Applications, Technical Digest (CD) (Optical Society of America, 2006), paper CFA3

[5] A. Ramaswamy, L. A. Johansson, J. Klamkin, H. Chou, C. Sheldon, M. J. Rodwell, L. A. Coldren, and J. E. Bowers, "Integrated Coherent Receivers for High-Linearity Microwave Photonic Links," J. Lightwave Technol. **26**, 209-216 (2008).

[6] T. Ishibashi, T. Furuta, H. Fushimi, S. Kodama, H. Ito, T. Nagatsuma, N. Shimizu, Y. Miyamoto, "InP/InGaAs Uni-Traveling-Carrier Photodiodes," *IEICE Trans. Electron.,* vol. E83-C, pp. 938-949, June 2000.

[7] Donato Pasquariello, E. Staffan Björlin, Daniel Lasaosa, Yi.-Jen Chiu, Joachim Piprek, and John E. Bowers, "Selective Undercut Etching of InGaAs and InGaAsP Quantum Wells for Improved Performance of Long-Wavelength Optoelectronic Devices," J. Lightwave Technol. **24**, 1470- (2006).

[8] E. J. Norberg , R. S. Guzzon , S. C. Nicholes , J. S. Parker and L. A. Coldren "Programmable photonic filters fabricated with deeply etched waveguides", *Proc. Int. Conf. Indium Phosphide and Related Materials*, pp. 163 2009.

[9] A. Ramaswamy *et al.*, "Demonstration of a Linear Ultra-Compact Integrated Coherent Receiver", submitted to MWP'10.

[10] Klamkin, J. " Coherent Integrated Receiver for Highly Linear Microwave Photonic Links ". Ph.D. dissertation, University of California-Santa Barbara, 2008.

[11] P .Yves Painchaud, Michel Poulin, Michel Morin, and Michel Têtu, "Performance of balanced detection in a coherent receiver," Opt. Express **17**, 3659-3672 (2009).